On the mass motions and the atmospheric states of moustaches(Dissertation_全文)

AUTHOR(S):

Kitai, Reizaburo

On the mass motions and the atmospheric states of moustaches

北井礼三郎

論文内容の要旨

報告番号	乙第　　号	氏名	北井礼三郎
論文調査担当者	主査　川口市郎 神野光男　小暮智一		

（論.文題目）

On the motions and the atmosperic states of mous-taches

（ムスタッシュの運動及び大気状態について）

（論文内容の要旨）

ムスタシュというのはHα線off－band単色像にみられる太陽活動領域のの中にある非常に小さな輝点であり、Hα線輪廓をみると中心波長領域ではみえないが、数Åに達する長い翼部が輝線として存在するのが特徴である。ムスタシュが物理的に如何なる現象であるかを理解するには、この巾広い翼部の解釈が重要である。従来の説明によれば、スタルク効果によってHα－輝線が拡るとか、あるいはムスタシュ大気には秒速数百kmに及ぶ運動があるとかいわれているが、定説がないのが現状である。

ムスタシュ現象の研究が発展しない理由の1つは輝点のサイズが1″程度あるいはそれ以下で極めて小さく正確な輝線輪廓の観測が困難なことによる。幸い近年飛騨天文台にドームレス太陽望遠鏡が新設され、時には1″あるいはそれ以下の微細構造を分解する良好な観測条件がえられることがある。申請者はこのドームレス太陽望遠鏡を用いて、極めて質の高いムス

タシュのスペクトルを撮影し，その解析にもとづいてムスタシュ現象に新しい解釈を提供している。

申請者によればムスタシュ Hα－輝線輪郭は次の3つの成分よりなっている。1.中心波長部分の強い吸収，2.中心波長と翼部の間（$\Delta\lambda = 0.5 \sim 1.0$ Å）のガウス状輝線部，3.翼部（$\Delta\lambda = 1.0 \sim 3.0$ Å）の羃状輝線部，また各成分の中心波長に対して青・赤両部分の輝線強度の比較から，この3つの成分は数*km*／ sec に及ぶ青側へのドップラー変位をもつことが判明した。

申請者は本論文において，以上の観測をムスタシュ大気に特有な源泉関数で説明した。即ち通常の太陽大気では温度・圧力の分布は種々の観測からくわしく知られており，この大気で生じる Hα－線は，この大気モデルにもとづく源泉関数を計算することによってその輪郭を説明することができる。もしムスタシュ大気が，ある擾乱によって通常の温度分布・圧力分布から変位し，さらにムスタシュ大気の上昇又は下降運動を考慮して，それに応じた源泉関数を計算すればムスタシュ大気から放射される Hα線輪郭が求まる。申請者は観測と理論の比較からムスタシュ大気内の温度・圧力にどの程度擾乱があるかを求めたのである。

申請者はまづ標準太陽大気モデルとして最も新しいＶＡＬ－Ｃのモデルを用いた。この大気について，4つのエネルギー準位をもつ水素原子モデルの非局所熱力学平衡状態における輻射輸達方程式をとき，源泉関数を求め，通常の Hα－線輪郭が充分再現できることを確めた。次いで申請者はこの標準大気モデルに種々の擾乱を与へ，この擾乱大気モデルから放射される Hα－線輪郭を求め，観測と比較した。その結果ムスタシュ大気内では彩層内の高さ 400～1200*km*の間の大気層で温度は1500K上昇し，かつ密度は標準大気の5倍であること．またドップラー速度については，この大気が擾乱域において徐々に加速上昇していると考えて観測をよく説明すると結論している。

ON THE MASS MOTIONS AND THE ATMOSPHERIC STATES OF MOUSTACHES

Reizaburo KITAI

Department of Astronomy, Faculty of Science,

University of Kyoto, Kyoto 606, Japan.

ABSTRACT

Analyses of broad moustache profiles of Balmer lines and Ca II H and K lines are performed based upon our spectroscopic observation under good seeing conditions. Hα emission profiles are found to consist of three components, i.e., a central absorption, a Gaussian core and a power law wing. Each of them has a different Doppler shift from others. From the data of Doppler shifts, mass motions with velocity of about 6 km/s are found to be present in chromospheric levels of moustache atmospheres. Computations of Hα emission profiles radiated from a variety of model atmospheres are made. Comparison of computed profiles with the observed ones leads us to the conclusion that a broad Hα profile is due to a formation of a heated ($\Delta T = 1500$ K) and condensed ($\rho / \rho_0 = 5$) chromospheric layers relative to the normal.

1. Introduction

Moustaches or Ellerman's bombs are characterized by their broad emission profiles. Basic data for the moustaches such as size, form, lifetime and associated phenomena have been revealed (Severny 1968, Engvold and Maltby 1968, Bruzek 1972, Roy and Leparskas 1973 and Kurokawa et al. 1982).

Although mass motions in moustache points are reported by the above cited authors and Kitai and Kawaguchi (1975), chromospheric velocity field has not yet been observed quantitatively. From our analysis of the observed Hα profiles of moustaches, we have found that mass motion with the velocity of about 6 km/s are present in chromospheric layers of moustaches directed generally upwards.

The broadening mechanisms of emission profiles were proposed by Engvold and Maltby (1968) and Severny (1968) Their mechanisms, however, were based upon very simplified atmospheric models and seem to be unable to explain the profiles totally Canfield and Athay (1973) computed the Hα profiles emitted from a flare model atmosphere constructed by Nakagawa et al. (1973) and showed the possibility of broad Hα emission from a heated and condensed atmosphere. In this paper, on the similar line of thought we have performed NLTE calculations on locally heated and condensed atmospheric models and the computed Hα profiles are compared with the observed ones. It is found that a formation of a hot ($\Delta T = 1500$ K) and dense ($\rho / \rho_0 = 5$) region in chromospheric layers can explain the observed broad Hα profiles.

In the final section, we discuss some possible sources of disturbances which give rise to the moustache phenomena.

2. Observations and reductions

An echelle spectrogram and six grating spectrograms are analysed in this work. The echelle spectrogram was taken at the Okayama Astrophysical Observatory on August 15, 1979. Characteristic broad emission components were observed in Hα, Hβ, Hγ and Hδ lines of nertral hydrogen and H and K lines of Ca II ion. The grating spectrograms were taken through the horizontal spectrograph of the Domeless Solar Telescope at the Hida Observatory on May 23, 1980. Six sharp Hα spectra of moustaches with spatial resolution of 1 - 2 arcsec were obtained. The dispersion of the spectrograms was 0.239 Å/mm at Hα Figure 1 shows the Hα spectra of the observed six moustaches. The emission components show a variety of profiles. Some moustaches have symmetrical emission profiles and the others have asymmetrical ones. From the analysis of these emission profiles we have derived the mass motion data in moustache atmospheres.

Figure 1

2.1 Reductions

Profiles of excess emission components of moustaches were obtained by subtracting spectra of neighbouring normal regions from moustache spectra. Although our observations were done under good seeing conditions, it was inevitable that the observed spectra were contaminated by the radiation from the neighbouring region. In this case, proper data for analysing moustache emissions are profiles of excess emission components, whose wavelength dependence is free from observational conditions. Thus in the following, analyses of observational data and

comparison with theoretical results are done on these profiles of excess emission components.

An emission component of a moustache can be decomposed into three sub-components. First one is a central absorption component, the second is a Gaussian emission core and the final is a power-law emission wing. This is true for all the observed profiles when we consider that these three components have mutually different Doppler shifts. For example, an emission profile of the moustache named No. 1, whose spectrum is shown in Figure 1, is displayed in Figure 2. Figure 2 (a) shows the excess emission component. This profile is not symmetrical about the line center. However when we consider that the profile is Doppler-shifted to the blue with a velocity of 5.8 km/s, the emission core ($\Delta\lambda' = 0.5 - 1.0$ Å) can be approximated by a Gaussian distribution as shown in Figure 2 (b) On the other hand, if we consider that the profile is Doppler-shifted to the blue with a velocity of 1.6 km/s, the emission wing part ($\Delta\lambda'' = 1.0 \quad 3.0$ Å) can be expressed by a power-law function. See Figure 2 (c) For another example, we take the moustache No. 4, which has a very asymmetrical emission profile. As can be seen in Figure 3, the emission wing part ($\Delta\lambda' = 1.0 - 2.0$ Å) can be expressed by a power-law function when the profile is assumed to be shifted to the blue with a velocity of 1.8 km/s.

Figure 2

Figure 3

Least square fitting to the emission profiles assuming a Gaussian form for the core and a power-law form for the wing gives us characteristics of emission components, which are summarized in Table 1 for the six moustaches. The second column of the table shows the intensity ratio between ΔI_b (the blue peak enhancement) and ΔI_r (the red peak enhancement) The forth, fifth and sixth columns indicate the Doppler shifts of central absorption components, Gaussian core components and power-law components respectively.

Table 1

Table 2

Table 2 gives the summary of our reduction for the moustache observed through the echelle spectrograph. As the wing part is very faint for this moustache, we can deduce only the characteristics of the Gaussian emission core parts for the lines Hα, Hβ, Hγ, Hδ and K.

2.2 Observational results

a) Asymmetry of emission profiles

The intensities of two peaks in a moustache emission profile are generally different. Blue asymmetry in the intensity peaks is known to be prevailing (Severny 1968) Statistical studies by Bruzek (1972) show a strong positive correlation between the red shift of central absorption components and the blue asymmetry of the intensity peaks. According to Bruzek, the central absorption components are produced by the overlying absorbing matter and the motion of the absorbing matter gives rise to the asymmetry in the peak intensities.

In our samples of six moustaches, the correlation found by Bruzek is confirmed to hold, except the moustache No. 1 and No. 3. The blue and red peak intensities are nearly the same in magnitude for the moustache No. 1, although the absorption component is Doppler-shifted to the blue (v = - 5.2 km/s) However this can be explained if we take into account of the Doppler shift of the Gaussian emission core. As the emission core and the central absorption are Doppler-shifted to the blue in nearly the equal velocities in this sample, the two peaks show nearly the same intensities in magnitude. For the moustache No. 3, we can see that the core component is shifted to the blue more than the absorption component and then the blue asymmetry arises.

We then propose that the asymmetry of peak intensities of a moustache is not only due to the motion of overlying absorbing matter but also due to the Doppler shift of the Gaussian emission core. This point will be discussed later after our theoretical NLTE calculations.

b) Motion of emitting regions

Based on the study of the ' Fraunhofer lines kink ', Severny (1968) reported the upward velocity field of 1 - 3 km/s at the photospheric levels in moustache atmospheres. At coronal heights, Roy and Leparskas (1973) observed a close spatial correlation between the moustaches and the fast moving (v = 100 km/s) dark elongated features and suggested that these dark features were ejected matter from the moustache points. Our observations reveal the velocity field at the chromospheric layers in moustache atmospheres.

As can be seen in Table 1, emission components are generally shifted to the blue and the shifts of the Gaussian core components are larger than those of the power-law wing components. We think that the Doppler shifts of the

components are due to the mass motions of the emitting regions. As the wing components are formed in lower layers than the core components, it seems natural to consider that matter in upper layers moves with a larger velocity than in lower layers. Table 2 supports this interpretation. Strong Hα and K lines which are formed in higher chromospheric levels show large Doppler shifts, while Hβ, Hγ and Hδ lines indicates little mass motion.

Combining our results with previous workers' observations, we conclude that matters in moustache atmospheres are not in static state and that they move faster in higher levels (i.e., 1 km/s at the photosphere, 6 km/s at the chromospheric layers and 100 km/s at the coronal heights) As the upward motion is generally observed in moustaches, we may say that moustaches are chromospheric manifestation of some ejection phenomena, i.e., small surges.

c) Profiles of emission components

The mechanism producing the wide emission profiles of moustaches is not yet known. The Doppler widths of Gaussian components expressed in velocity units ranges from 70 km/s to 100 km/s. See Table 2. As these values exceed the chromospheric sound velocities, it is hard to consider that these large Doppler widths are due to non-thermal microturbulent motions. On the other hand, the indices of power-law functions fitting the wing profiles ranges from - 1.6 to - 2.5. So simple explanations with the Stark effect cannot be applied.

To explain the profiles of emission components, a new mechanism is needed. Our proposal for the mechanism is given in the next sections based upon the results of our NLTE calculations.

3. NLTE calculations

In order to get insight into the atmospheric state of moustaches, we have performed non-LTE calculations and derived theoretical Hα emission profiles for a variety of model atmospheres. Comparing the observed profiles with theorerical ones, we have found that there exist temperature and density enhancements at the chromospheric levels in a moustache atmosphere and that due to these enhancements broad moustache emissions are produced.

3.1 Procedure of calculations

a) Method

NLTE calculations for theoretical Hα profiles are performed in two steps.

In the first step, we solve the radiative transfer equations coupled with the statistical equlibrium equations with the complete linearization method formulated by Auer and Heasley (1976) As the hydrogen atom is the principal electron contributor in the chromosphere, ionization balance equation is included in the calculation. In this step of calculation for excitation and ionization state of hydrogen atoms, only Doppler broadening due to thermal plus small-scale non-thermal motions is taken into account as the line broadening mechanism. And complete frequency redistribution for the line photon scattering is assumed. The assumption of complete redistribution in Doppler core neglecting the wing is a good approximation in calculating the source functions (i.e., level population fields), as was stated in Milky and Mihalas (1973)

In the second step, theoretical Hα profiles are derived by using the level population obtained in the previous step. In this step all the broadening mechanisms such as Doppler, natural, resonance and Stark broadening are included.

For resonance broadening we use the result of Ali and Griem (1965, 1966) For Stark broadening we refer the work of Griem (1960) As the Fourier transform of the Voigt profile can be done analytically, the convolution of the Voigt profile with the Stark profile is performed numerically using the Fourier transform technique.

When we introduce some macroscopic velocity fields into our model atmospheres, the effects of velocity fields are neglected in the first step of calculations. The Doppler shift of absorption profile is taken into account only in the second step. The validity of this treatment of the effects of macroscopic velocity fields is confirmed by Canfield and Athay (1974) on the flare model atmospheres, especially when the amplitude of the velocity field is less than 20 km/s.

b) Model atmosphere and model atom

We adopt the VAL-C model as the unperturbed model atmosphere (Vernazza, Avrett amd Loeser 1981), which is the most recently published and is plane-parallel and in hydrostatic equilibrium. Perturbed model atmospheres are constructed by increasing temperature and / or density values for given height ranges. Distributions of temperature and density enhancements through the height are displayed schematically in Figure 4. In this paper we assume that the enhancements in temperature and density occur in common height ranges. As the temperature perturbation and the density enhancement are introduced in mutually independent way, it should be noted that our perturbed model atmospheres are not in hydrostatic equilibrium. The microturbulent velocity field in a perturbed model atmosphere is assumed to have the same distribution as the VAL-C. Calculations are done for 51 depth-mesh points in the range -75 km $\sim +2543$ km measured from $\tau_{5000} = 1$ level.

Figure 4

Our model hydrogen atom consists of three bound levels and one continuum. Cross-sectional data for collisional ionization, photoionization and collisional excitation are calculated using the subroutines in ' LINEAR ' code published by Auer, Heasley and Milky (1972) Reference is made to Allen's ' Astrophysical Quantities ' for the oscillator strength of hydrogen line transitions. Transfer equations are solved for all lines and continua of the hydrogen atom. In solving the level populations, 10 equally separated frequency mesh points that cover the region from line center to the frequency displaced by five times the thermal Doppler width for T = 10000 K are used for each line. For each continuum, 8 mesh points, which correspond to the Gaussian quadrature points, are selected.

c) Opacity

As the continuum opacity sources, we include electron scattering, H^- b-f and f-f transitions, CI b-f transitions, SiI b-f transitions, MgI b-f transitions and HI b-f and f-f transitions. The cross-sections of these transitions are calculated following ' LINEAR ' code. H^- molecules and metal atoms are treated as if they are in LTE state. Opacities in the UV wavelength region due to numerous line absorptions are treated in a rough approximation by adding 50 times the metal continuum opacity in the wavelength region $\lambda\lambda$ = 2000 - 4000 Å (Vernazza et al. 1981).

3.2 Results of calculations

We have performed the NLTE calculations on 11 atmospheric models whose charactertistics are tabulated in Table 3 and displayed in Figure 5 and Figure 11.

Table 3

Figure 5

General features of the effects of the temperaute and / or the density enhancements on the Hα line profiles can be drawn from the results for four atmospheric models indicated in Figure 5. Line source functions and line-center optical depths for the Lyα, Lyβ and Hα lines are shown in Figure 6. Hα profiles for each model atmosphere are illustrated in Figure 7, where profiles computed for five different view-angles ($1/\cos\theta$ = 1.0,2.0,5.0,10.0 and 20.0) are drawn.

Figure 6

Figure 7

Results can be summarized in the following:

a) The moustache emission can appear only if the temperature enhancement is present.

Characteristic double peaked Hα emissions don't appear in the density enhanced model T0R5, but can be seen in the temperature enhanced models T1R0 and T1R5. Double peaked emissions can be produced when the source functions are not monotonously decreasing along the height but have local peaks in the chromospheric levels. As can be seen in Figure 6, local chromospheric heatings do enhance the chromospheric Hα source functions.

The solar Hα line is known to be photoelectrically controlled line, whose source function is insensitive to the temperature rise in the chromosphere (Thomas 1957, Athay 1972) However the photoionization rate in the Balmer continuum (2×10^{4} s^{-1}) is not so large compared with the collisional excitation rate (5×10^{3} s^{-1}) in the chromosphere (Athay 1972) When the collisional excitation rate is enhanced by some additional heating, the Hα line turns to be collisionally controlled. Thus a local chromospheric heating gives rise to the enhancement of the Hα source function. Canfield and Athay (1974) have shown the similar response of the Hα source function to the atmospheric heating for realistic flare models.

b) When the temperature enhancement is present, an additional density enhancement promotes the visibility of moustache emissions.

As is seen in Figure 7, the visibility of moustache emission in the model T1R5 is higher than that in the model T1R0. The difference between two models is due to the existence of an additional density enhancement. This point can be understood in the following way. In Figure 8, the total (line + continuum) source functions and the formation regions for three frequencies, i.e. line-center, inner wing and outer wing frequencies, are displayed for the model T1R0. An additional density enhancement has the effect to increase the Hα opacity and

then to rise up the formation regions. Thus at the wing frequencies radiations are formed at the regions where the source functions have higher values.

Figure 8

By the way, based upon the comparison of Hα line center optical depth distributions of the two model T0R0 and T1R0, it should be noted that the temperature enhancement itself has the effect to enhance the Hα opacity relative to the unperturbed atmosphere. This effect also contributes to the higher visibility of the emission (Canfield and Athay 1974)

c) Center to limb brightening of peak intensities.

Our model calculations show an interesting property that peak intensities of a moustache are higher when the distance of the moustache point from the disk center becomes larger (Figure 7) In other woeds, we can observe moustaches with more contrast as we go near the limb. This property can be explained with the same arguments as in 3.2 b) if we note that when we see the object near the limb at one frequency, we observe the radiation formed at higher levels compared to the object at the disk center

Although this property does not seem to contradict our observational impression, it would be necessaty to be checked quantitatively by a future statistical study. Engvold and Maltby (1968) noted a slight limb-brightening trends in their observational data.

d) Center to limb variation of peak separation.

Figure 7 shows that the wavelength separation between two peaks is a monotonously increasing function of $\cos\theta$ In other words, the peak separation of a moustache near the limb is larger than that of a moustache at the disk center. Explanations of this property can be given with the reference to Figure 8. At the core frequencies, the source functions are decreasing functions of height near the formation depths. So the brightness decreases from the center of the disk to the limb at these frequencies. On the other hand, the source functions are increasing functions of height near the formation depths of the inner wing frequencies ($|\Delta\lambda| \geq 1$ Å). So the brightness increases from the center to the limb at the inner wing frequencies. This difference of the center-to-limb brightness variation between the core and the wing frequencies gives rise to the center-to-limb variation of the peak separation.

This theoretically predicted property must be confirmed observationally, although observational confirmation seems to be very difficult because the peak intensity is highly influenced by the overlying absorbing matter or the mass motions discussed in the next subsection.

e) Effect of mass motions

Mass motions in the chromospheric layers have a great effect on the Hα emission profiles. The effects of mass motions are examined by two representative mass motion models. Two models of velocity distribution with height are illustrated in Figure 9. The direction of motion is assumed to be vertically upwards. In the mass motion model V1, the mass motions occur locally in the temperature and / or the density enhanced region, or in the highly-excited region. On the other hand, in the mass motion model V2, the upper chromospheric layers are also

in motion in addition to the lower chromospheric motions. We have adopted these velocity models for study because they represent schematically the velocity fields when a hydrodynamic shock wave propagates outwards from the photosphere to the corona. The model V1 represents the velocity field when the shock is propagating in the chromosphere and the model V2 represents the velocity field when the shock has passed through the chromosphere (Suematsu et al. 1982).

Figure 9

The Hα profiles when the velocity fields are taken into account are shown in Figure 10. The Hα profiles computed for the static T1R5 atmosphere and for the unperturbed T0R0 atmosphere are also shown in the figure for reference. The results at two θ positions are shown in the figure.

Figure 10

As can be expected from the velocity field profiles, the Hα profiles are influenced only in the inner wing and in the core part, and the form of outer wings remains unchanged. When a local motion in the high excitation region is present, the emission profile show a blue asymmetry. However, when upper layers are also in motion with larger velocities, the core part is shifted to the blue further and the emission profile becomes to show a red asymmetry.

Thus the asymmetry of Hα profiles is controlled by the profile of the velocity field in the chromosphere. We have made use of this effect to derive the chromospheric velocity data from our observed Hα profiles.

If a hydrodynamic shock passage is the origin of a moustache, our computation suggests that the asymmetry of the Hα profile would be observed to change from the blue to the red along time.

Mass motions in moustache atmospheres have another interesting effect on the Hα profiles. As is seen in Figure 10, when the atmosphere is in motion the peak intensity is higher than that when the atmosphere is static. This effect can be explained by the optical depth change in the inner wing due to mass motions, because the radiation emitted in the inner wing get stronger when the optical depth becomes larger as discussed previously In interpreting the brightness variations of moustaches or flares observed in filtergrams, the variation of velocity fields must be taken into account due to the effect described above (Kurokawa et al. 1982).

3.3 Comparison with observations

Although the results of the four atmospheric models discussed in 3.2 tell us the generel features of the Hα emissions from perturbed atmospheres, computed Hα profiles for these models do not fit the observed ones. In particular, the profile computed for the T1R5 model at very small μ position shows extremely bright continuum enhancement ($\Delta I = I_{\text{normal continuum}}$) which is not observed. To avoid this difficulty, computations for a new series of models (model A - G) are performed by assuming that the perturbations in the temperature and density occur in higher region than the previous four models (Table 3) Possible model atmospheres which explain the observed Hα profiles are searched in these new models.

Figure 11

In Figure 12, theoretical emission profiles computed for models A - G at $\mu^{-1} = 2.0$ and $\mu^{-1} = 5.0$ are illustrated. The theoretical profiles in this figure are those of excess emissions from the unperturbed profile. As stated previously, this is because of our aim of the proper comparison with the observed profiles. It should be noted that the theoretical profile has a Gaussian form in the inner wing and a power-law form in the outer wing for the models where the temperature and the density enhancement are large (model D, F and G) This characteristics is strengthened as μ^{-1} increases.

Figure 12

In Figure 12 (a), the emission profile of the moustache No 1 which was observed at $\mu^{-1} = 1.4$ is plotted. The observed profile fits the theoretical one computed for the model F in the wavelength region of $\Delta\lambda = 0.8 - 3.0$ Å. In other words, the Gaussian part and the power-law part of the observed profile match the theoretical profile.

For the moustache No. 5 ($\mu^{-1} = 3.4$), the comparison with the theoretical profiles is shown in Figure 12 (b) Either the model C or the model E explains the observation in this sample.

A word of comment is given on our fitting procedure. Considering the seeing effect, we must regard our observed intensities of emission components as the lower-limit of the real emissions. If the observations were done with perfect spatial resolution, the intensities of emissions would be higher. So we must search the best-fit theoretical profiles among those which have larger absolute intensities than the observed emission. For this reason, the model A and the model B are rejected in searching the model atmosphere for the moustache No. 5.

The results of our fitting for all the observed profiles are shown in Figure 11 where the model atmospheres selected for the observed profiles are indicated in ΔT - ρ/ρ_0 diagram with their code numbers. This figure gives us our main conclusion that moustache emissions are emitted when dense and hot regions are formed in the chromosphere (h = 700 - 1200 km). The temperature enhancements required are about 1500 K. The density must be increased by a factor of about five relative to the undisturbed atmosphere.

4. Discussions

Mechanisms which explain the broad emission profiles of moustaches have been proposed thus far by many authors. Simple arguments which explain the broadening by a supersonic non-thermal motion have been unsuccesful because it is hard to confine the high-velocity material in a small region for the lifetime of a moustache.

Engvold and Maltby (1968) discussed two possible mechanisms. First one is that broad profiles are due to macroscopic motions (v = 200 km/s) in filamentary daughnut-shaped channels oriented more or less at random directions. Although Gaussian emission components may be explained by this mechanism, power law components cannot be explained. The driving and maintaining mechanisms of the supersonic motions in the special geometry for the lifetime of a moustache were not made clear. As another possible source of the broadening, they suggested the effect of electron scattering. They argued that when the atmosphere is heated, sufficient electrons are supplied due to enhanced ionization of hydrogen atoms and that scatterings by electrons broaden the profile. Following their estimates, an electron density $n = 10^{16}$ cm^{-3} along 1000 km is required to influence the line profile. However we cannot think that a hot and dense region like this is really formed because the particle density in recent model atmosphere (Velnazza et al. 1981) can take 10^{16} cm^{-3} only in a deep depth (h = 350 km) If the hydrogen atoms above the temperature minimum were fully ionized, the electrons would by insufficient to influence the line profile.

Severny (1968) suggested a mechanism that the line broadening is due to incoherent scattering in expanding opaque layer. He computed the profile of outcoming radiation from a homogeneous ($n_2 = 10^7$ cm^{-3}), isothermal ($T = 10^4$ K) and opaque ($\tau_{H\alpha} = 95.56$) layer According to his results, his model can

explain the intensity distribution, the blue asymmetry and the central gap of the Hα emission profile under reasonable assumptions. His computations, however, were done on very simplified model. Although moustache points are situated in the chromosphere (Bruzek 1972). he selected only the disturbed region and treated the region as if isolated from overlying or underlying atmospheres. So his model may be applied to some limb phenomena but does not seem to be applicable to the moustache on the disk. In particular, the central gap of the Hα profile is not formed as his model predicts, but is due to the effect of overlying matter as Bruzek's (1972) and our works have shown. Although Severny's results cannot be accepted fully, they support our results partially by the fact that his computed profiles match the observed ones in the wing part because his and our methods of analysis become essentially the same in the wavelengths where the chromosphere is optically thin. We consider that his success in explaining the broad profile is the result of his assumptions of rather high temperature and of specific form of source function distributions.

In our opinions, the line broadening is neither due to electron scattering nor due to the expanding motion but simply due to the heating with some compression of the lower chromosphere. Local source function increment due to the heating results in the broad line profiles.

Next we discuss the atmospheric and hydrodynamic state of moustache points. Our observations and computations show that a hot (ΔT = 1500 K) and dense (ρ/ρ_0 = 5) region is formed and the matter is in motion (v = 6 km/s) generally directed upwards in the chromospheric layers of a moustache points.

Kurokawa et al. (1982), following the evolution of moustaches in filtergrams showed that a moustache has a spike-like form and grows in length in the brightening phase. The mean upward velocity of 8 km/s was reported. Their

results on the dynamical features of moustaches agree well with the results of our spectroscopic study.

The temperature enhancement required in our model has the similar value as the temperature excess in the plage chromosphere relative to the normal chromosphere (Shine and Linsky 1974) On the other hand, the density in our moustache model is higher than the plage model about 7 times. Thus we can think that an isothermal compression or an isothermal vertically propagating shock wave in the pre-heated plage chromosphere gives rise to a moustache atmosphere. As the moustache points are observed associated with continuum facular granules (Severny 1968, Bruzek 1972), this line of speculations seems to be promising.

In this respect, it is interesting to refer the results of numerical simulations on the spicule ejection performed by Suematsu et al. (1982). They studied the vertical propagation of shocks produced by some impulsive heating at the normal photosphere or at the normal chromosphere. Under the assumption of nearly isothermal shock propagation, they followed the evolution of a shock produced by an initial abrupt pressure enhancement at h = 360 km. According to their results, the density at h = 1360 km is increased about ten times at maximum. And the chromospheric matter are forced in motion with the velocity of 12 km/s at maximum. Thus similar hydrodynamic models based on the plage atmosphere seems to explain the formation of the moustache atmosphere.

Interesting results of Suematsu et al. (1982) is the recurrent formation and upward propagation of shock waves. This behavior of the model may correspond to the recurrent brightening of a moustache observed by McMath et al. (1960) and Kurokawa et al. (1982)

By the way, if the shock propagation through the chromosphere is the origin of a moustache, our model predicts that the asymmetry of the Hα emission peaks

changes from the blue to the red along time as stated in 3.2 e), at least in initial phase. Similar change of Hα emission asymmetry is reported for flare kernels (Svestka 1976), though in this case the asymmetry is not of peak intensity but of profile itself. Taking into account of the velocity effect on the Hα profile, we may think that a shock wave propagates in a flare kernel because the direction of the chromospheric velocity predicted by the model of Suematsu et al. (1982) change from upward to downward.

Finally, we propose future observational and theoretical works to be done for the understanding of the moustache phenomena. Simultaneous spectroscopic observations of the evolution of moustache points in continuum brightness, in faint Fraunhofer lines and in Hα line are highly needed. From the analysis of these observations, the atmospheric states in moustaches from the photosphere to the chromosphere will be made clearer. In particular, comparison of the brightness variation between the continuum and the lines will give us the information on the propagation of disturbances which give rise to the moustache phenomena. Our computations are done on plane-parallel one-dimensional atmosphere, although a moustache has a spike-like three-dimensional form (Kurokawa et al. 1982). The source function enhancement due to disturbances will be lower than our results if we take into account of the three-dimensional geometry. The temperature or the density enhancements obtained in this paper may be the lower limit. NLTE calculations including three-dimensional effects will be necessary to perform more quantitative analysis on the moustache.

Ackowledgements

The autor would like to thank Prof. I. Kawaguchi for his valuable discussions and continuous encouragement. He is also grateful to all the staff members of the Okayama Astrophysical Observatory, University of Tokyo for their assistance in the observations. He expresses his hearty thanks to all the staff members of the Hida Observatory, University of Kyoto for their guidance in the spectroscopic observations with the Domeless Solar Telescope and for the fruitful discussions with them. Numerical computations were carried out on the FACOM M-200 at the Data Processing Center, Kyoto University.

REFERENCES

Ali, A.W. and Griem, H.R.: 1965, Phys. Rev. 140A, 1104.

Ali, A.W. and Griem, H.R.: 1966, Phys. Rev. 144, 366.

Allen, C.W.: 1973, 'Astrophysical Quantities', Athlone Press, London.

Athay, R.G.: 1972, 'Radiation Transport in Spectral Lines', D. Reidel Publ. Co., Holland, pp 86 91.

Auer, L.H., Heasley, J.N., and Milky, R.W.: 1972, A Computational Program for the Solution of Non-LTE Transfer Problems by the Complete Linearization Method (Kitt Peak National Observatory Contribution No. 555)

Auer, L.H. and Heasley, J.N.: 1976, Ap. J. 205, 165.

Bruzek, A.: 1972, Solar Phys. 26, 94.

Canfield, R.C. and Athay, R.G.: 1974, Solar Phys. 34, 193.

Engvold, O. and Maltby, P.: 1968, in Y. Öhman (ed.), 'Mass Motions in Solar Flares and Related Phenomena', Nobel Symp. 9, 71.

Griem, H.R.: 1962, Ap. J. 136, 422.

Kitai, R. and Kawaguchi, I.: 1975, Solar Phys. 44, 403.

Kurokawa, H., Kawaguchi, I., Funakoshi, Y. and Nakai, Y.: 1982, Solar Phys. 79, 77.

McMath, R.R., Mohler, O.C. and Dodson, H.W.: 1960, Proc. Nat. Acad. Sci. U.S. 46, 165.

Milky, R.W. and Mihalas, D.: 1973, Ap. J. 185, 709.

Nakagawa, Y., Wu, S.T and Han, S.M.: 1973, Solar Phys. 30, 111.

Roy, L.-R. and Leparskas, H.: 1973, Solar Phys. 30, 449.

Shine, R.A. and Linsky, J.L.: 1974, Solar Phys. 39, 49.

Severny, A.B.: 1968, in Y. Öhman (ed.), 'Mass Motions in Solar Flares and Related Phenomena', Nobel Symp. 9, 71.

Suematsu, Y., Shibata, K., Nishikawa, T and Kitai, R.: 1982, Solar Phys. 75, 99.

Svestka, Z.: 1976, 'Solar Flares', D. Reidel Publ. Co., Holland, pp. 76 - 80.

Thomas, R.N.: 1957, Ap. J. 125, 260.

TABLE 1.

H-alpha emission characteristics of the 6 moustaches

No.	$\Delta I_b / \Delta I_r$	Asymmetry	v(abs.)	v(core)	v(wing)
1	1.08	none	-5.2 (km/s)	-5.8 (km/s)	-1.6 (km/s)
2	1.16	blue	+4.4	-0.2	-1.7
3	1.30	blue	-2.0	-5.9	-1.7
4	3.48	blue	+26.6	?	-1.8
5	0.71	red	-6.4	?	-2.5
6	0.92	none	-1.6	-2.6	-2.1

TABLE 2.

Doppler shifts and Doppler widths of the emission cores for the Balmer and K lines (unit : km/sec)

line	v(shift)	v(width)
K	+ 8.2	67.7
Hα	+10.2	98.7
Hβ	- 0.4	89.7
Hγ	+ 0.4	87.3
Hδ	- 0.9	73.2

TABLE 3.

Parameters of the 11 model atmospheres

Model	h_1 (km)	h_2 (km)	ΔT (K)	ρ/ρ_o
T0R0	400	1200	0	1
T0R5	400	1200	0	5
T1R0	400	1200	1000	1
T1R5	400	1200	1000	5
A	700	1200	500	5
B	700	1200	1000	1
C	700	1200	1000	5
D	700	1200	1000	10
E	700	1200	1500	1
F	700	1200	1500	5
G	700	1200	1500	10

Figure Captions

Figure 1. : H_α spectra of the six moustaches observed through the horizontal spectrograph of the Domeless Solar Telescope at the Hida Observatory.

Figure 2. : H_α excess emission profile of the moustache No. 1. (a) Excess emission profile ($\Delta I / \Delta I_0$) is drawn against the wavelength separation from the line center ($\Delta\lambda$) where I_0 is the intensity of the continuum. (b) log I vs. ($\Delta\lambda'$)$^{\frac{3}{2}}$ plot of the profile. (c) log ΔI vs. log $\Delta\lambda''$ plot of the profile. $\Delta\lambda'$ and $\Delta\lambda''$ are the wavelength separations measured from the line centers which are shifted with the velocity of the core component and with that of the wing component respectively. Filled circles indicate the profile in the shorter wavelength region and open circles indicate the profile in the longer wavelength region.

Figure 3. : The same as in Figure 2 but for the moustache No.4.

Figure 4. : Schematic drawing of the atmospheric disturbances relative to the unperturbed atmosphere. (a) The temperature enhancement. (b) The density enhancement. ρ and ρ_0 are the density values of the perturbed and the unperturbed atmospheres respectively.

Figure 5. : Model atmospheres in ΔT vs. ρ / ρ_0 plane.

Figure 6. : Line source functions (S) and line center optical depths ($\bar{\tau}$) of the Ly_α, Ly_β and H_α lines for the models (a) T0R0, (b) T0R5, (c) T1R0 and (d) T1R5. The unit of the source functions is ergs/(cm^2 sec - sr Hz).

Figure 7. : Hα profiles emitted from the model atmospheres (a) T0R0, (b) T0R5, (c) T1R0 and (d) T1R5. $1/\mu$ (= $1/\cos\theta$) value is labelled for each profile.

Figure 8. : Total source functions and optical depths at three representative wavelengths in the Hα profile emitted from the model atmosphere T1R0. Source functions and optical depths at $\Delta\lambda$ = 0.0 Å, 1.0 Å and 5.0 Å are, respectively, indicated by S0 and TAU0, S1 and TAU1 , and S5 and TAU5.

Figure 9. : Schematic drawing of the velocity fields. (a) The velocity model V1. (b) The velocity model V2.

Figure 10. : Effect of the velocity field on the Hα profiles. The basic model atmosphere is T1R5. Thick curve indicates the profile when the atmos-atmosphere is static. Dot-dashed curve and dashed curve show, respectively, the profiles when there exist the V1 velocity field and when there exist the V2 velocity field. Dotted curve shows the unperturbed normal profile. (a) Hα profiles at the disk center (θ = 0.0). (b) Hα profiles near the limb (θ = 78.5°).

Figure 11. : Model atmospheres (A-G) in ΔT vs. ρ/ρ_0 plane. The model atmospheres which explain the observed Hα profiles (No. 1 No. 6) are also indicated by their code numbers.

Figure 12. : Hα excess emission profiles computed for the model atmospheres A - G compared with the observations. Computed profiles are shown only for inner and outer wings and central absorption profiles are not shown. (a) $1/\mu$ = 2.0. Observed profile for the moustache No. 1 are plotted with circles (b) $1/\mu$ = 5.0. The same as (a) but for the moustache No. 5.

Figure 1

H-alpha spectra of moustaches

→ λ

Figure 2

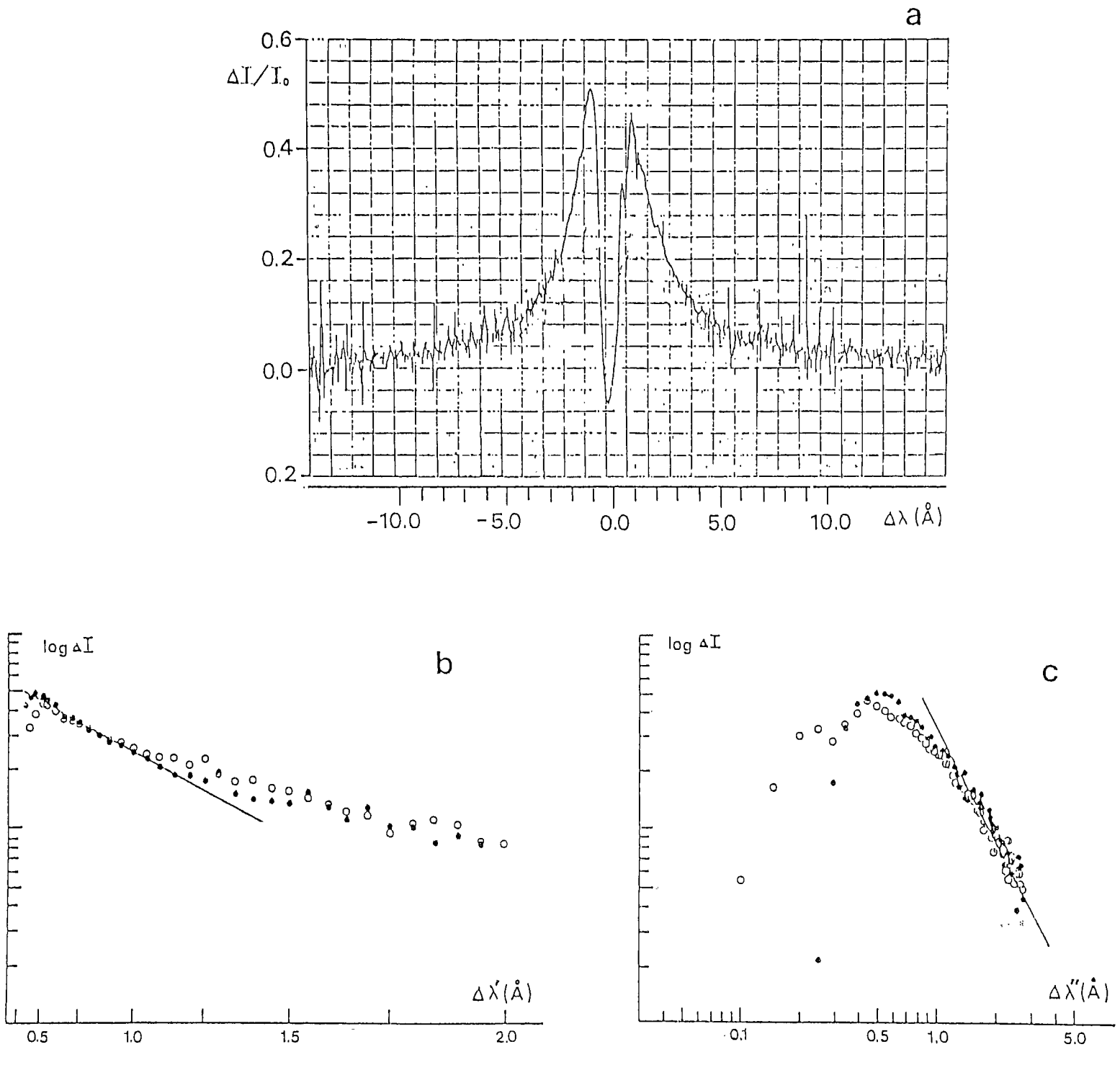
a
0.6
ΔI/I₀
0.4
0.2
0.0
0.2
-10.0
-5.0
0.0
5.0
10.0
Δλ (Å)
log ΔI
b
Δλ'(Å)
0.5
1.0
1.5
2.0
log ΔI
c
Δλ''(Å)
0.1
0.5
1.0
5.0

Figure 3

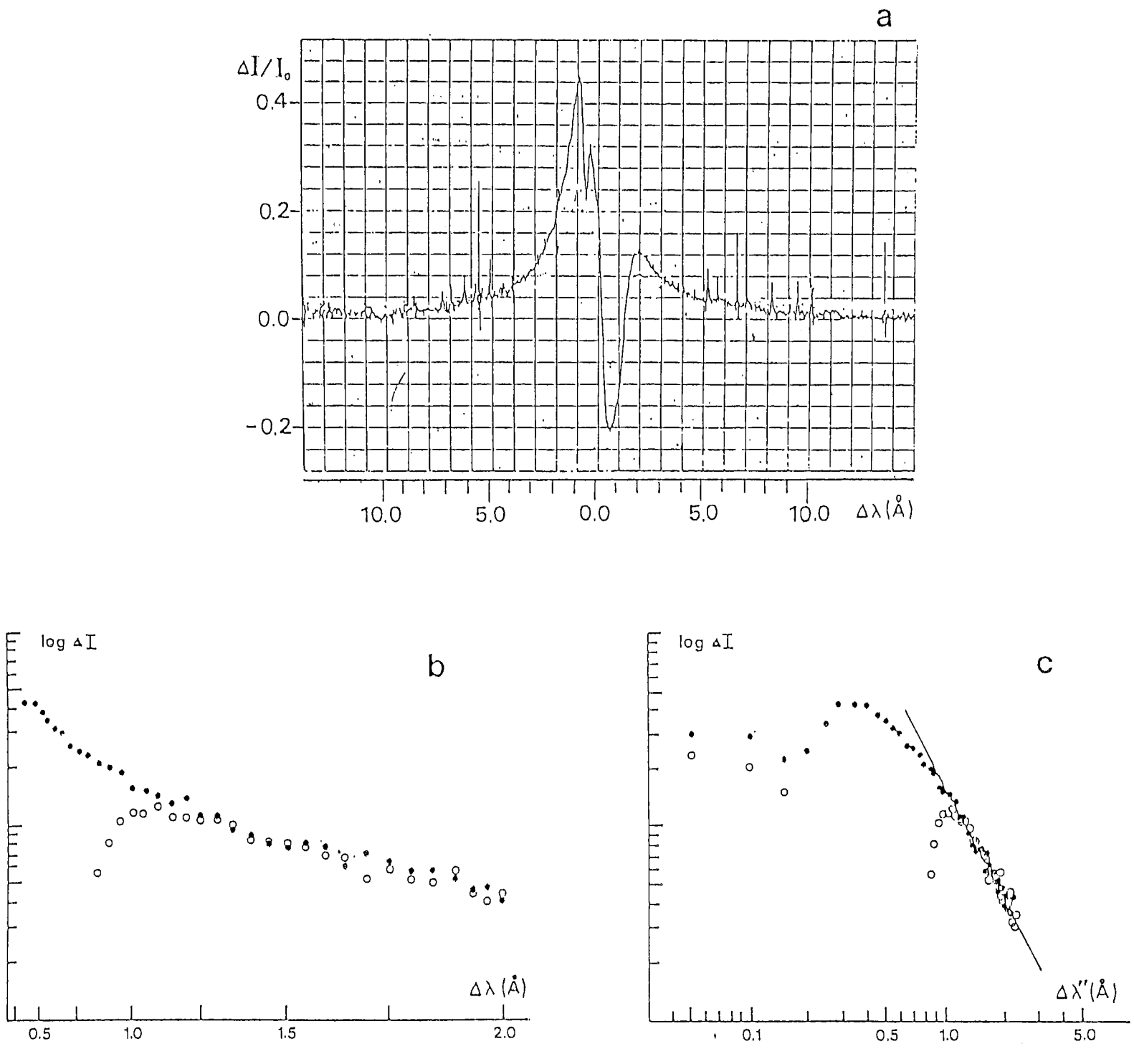
a
ΔI/I₀
0.4
0.2
0.0
-0.2
10.0
5.0
0.0
5.0
10.0
Δλ(Å)
log ΔI
b
Δλ (Å)
0.5
1.0
1.5
2.0
log ΔI
c
Δλ''(Å)
0.1
0.5
1.0
5.0

Figure 4

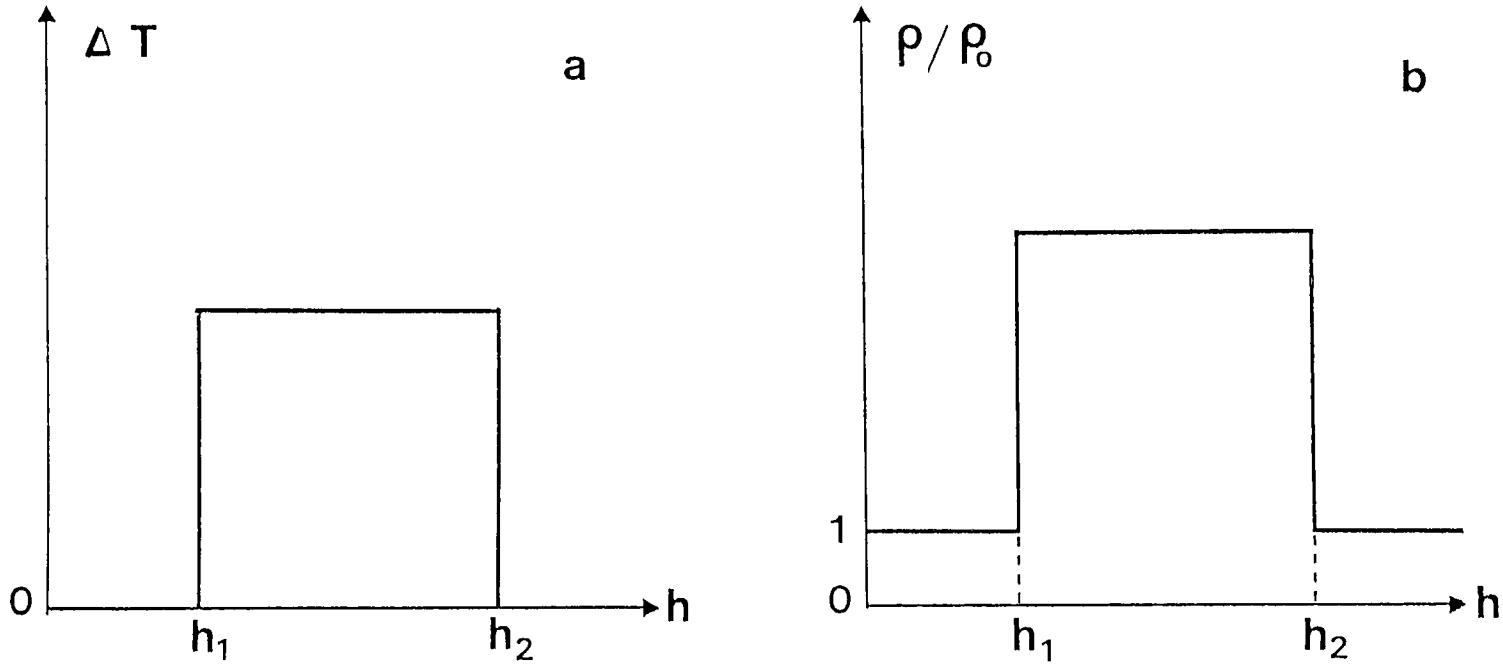

Figure 5

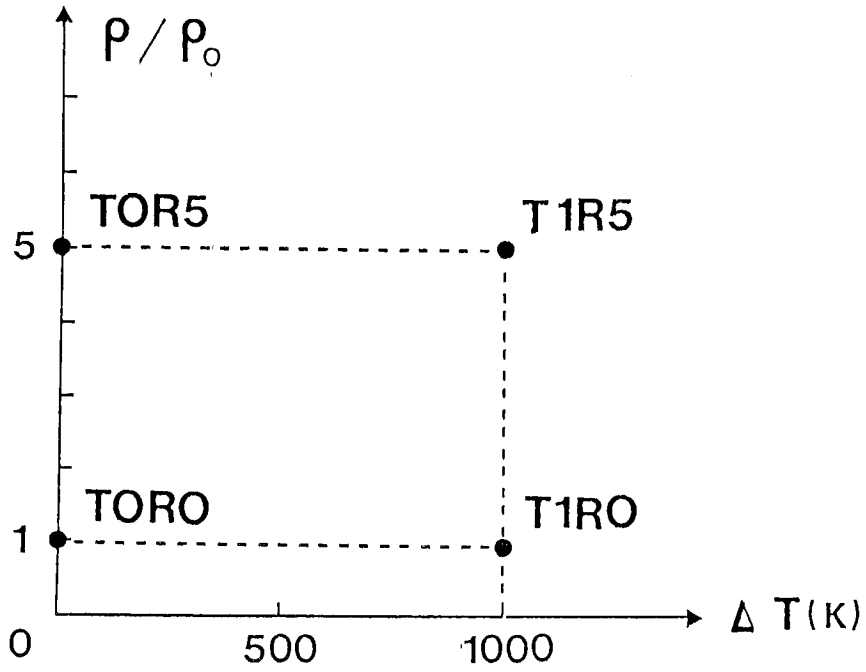

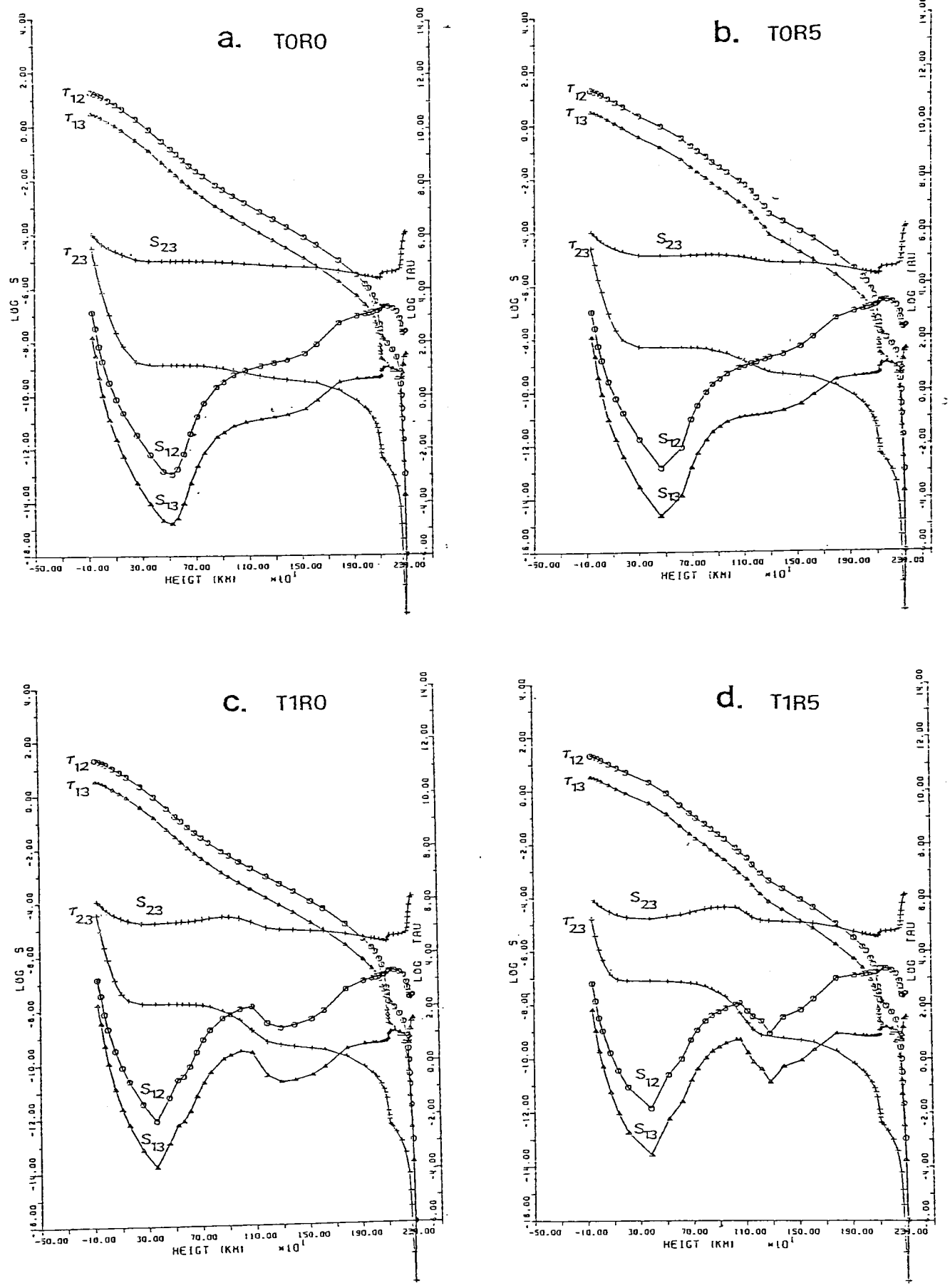
a. T0R0
b. T0R5
c. T1R0
d. T1R5
T_{12}
T_{13}
T_{23}
S_{23}
S_{12}
S_{13}
LOG S
LOG TAU
HEIGT (KM) ×10³

Figure 6

Figure 7

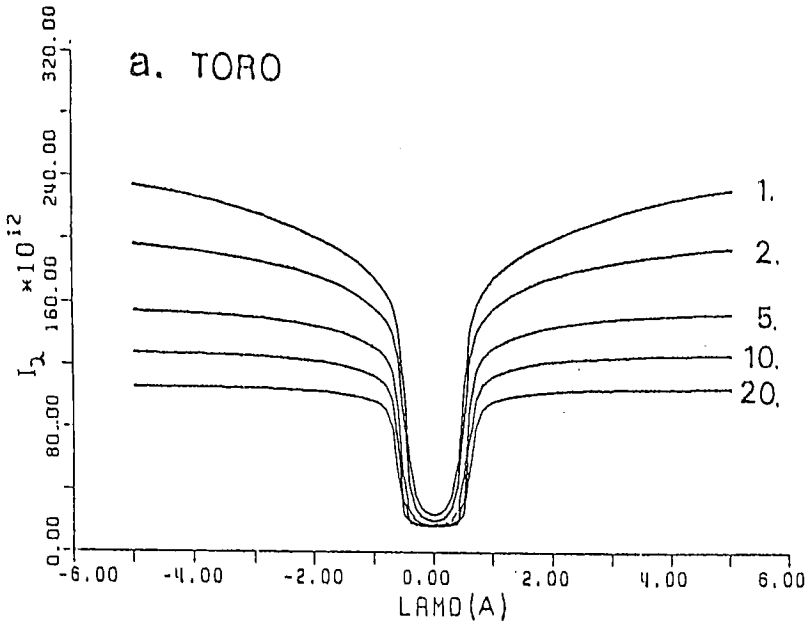
a. TOR0
I_λ *10^12
320.00
240.00
160.00
80.00
0.00
-6.00
-4.00
-2.00
0.00
2.00
4.00
6.00
LAMD(A)
1.
2.
5.
10.
20.

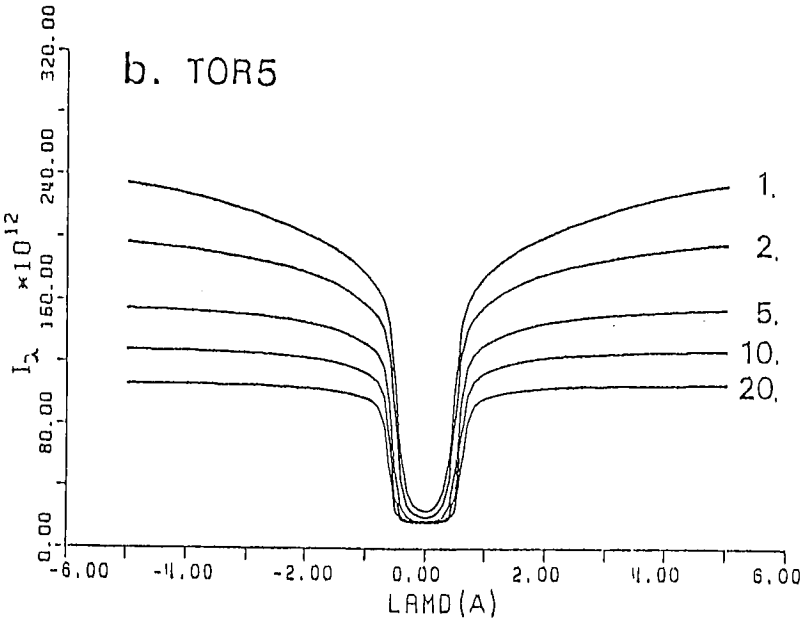
b. TOR5
I_λ *10^12
320.00
240.00
160.00
80.00
0.00
-6.00
-4.00
-2.00
0.00
2.00
4.00
6.00
LAMD(A)
1.
2.
5.
10.
20.

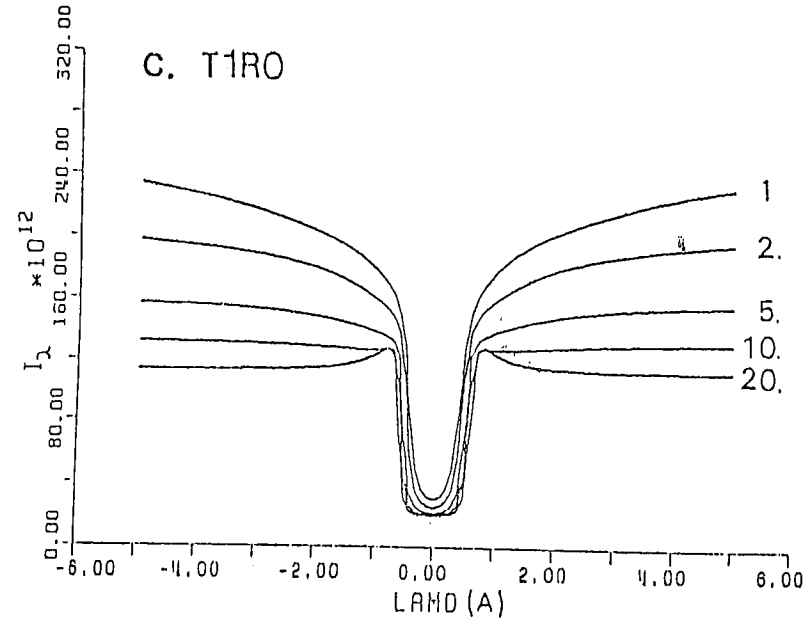
c. T1R0
I_λ *10^12
320.00
240.00
160.00
80.00
0.00
-6.00
-4.00
-2.00
0.00
2.00
4.00
6.00
LAMD(A)
1
2.
5.
10.
20.

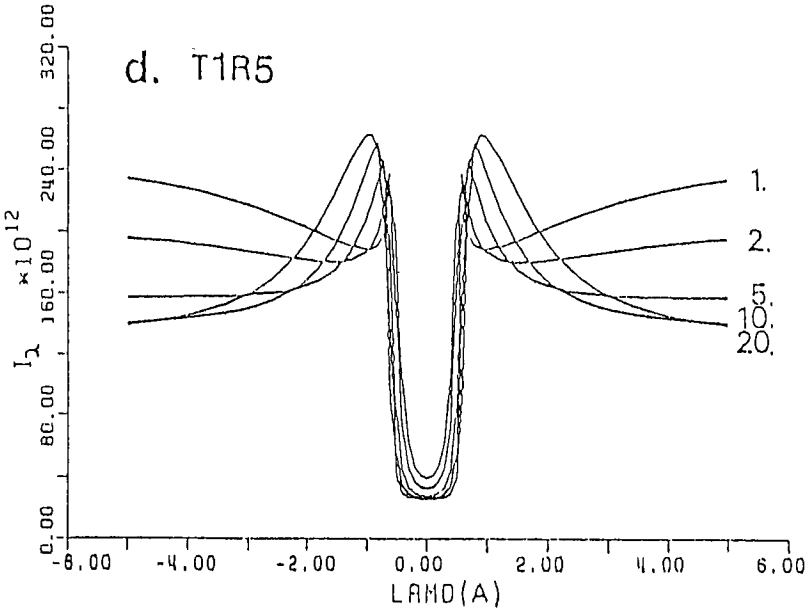
d. T1R5
I_λ *10^12
320.00
240.00
160.00
80.00
0.00
-6.00
-4.00
-2.00
0.00
2.00
4.00
6.00
LAMD(A)
1.
2.
5.
10.
20.

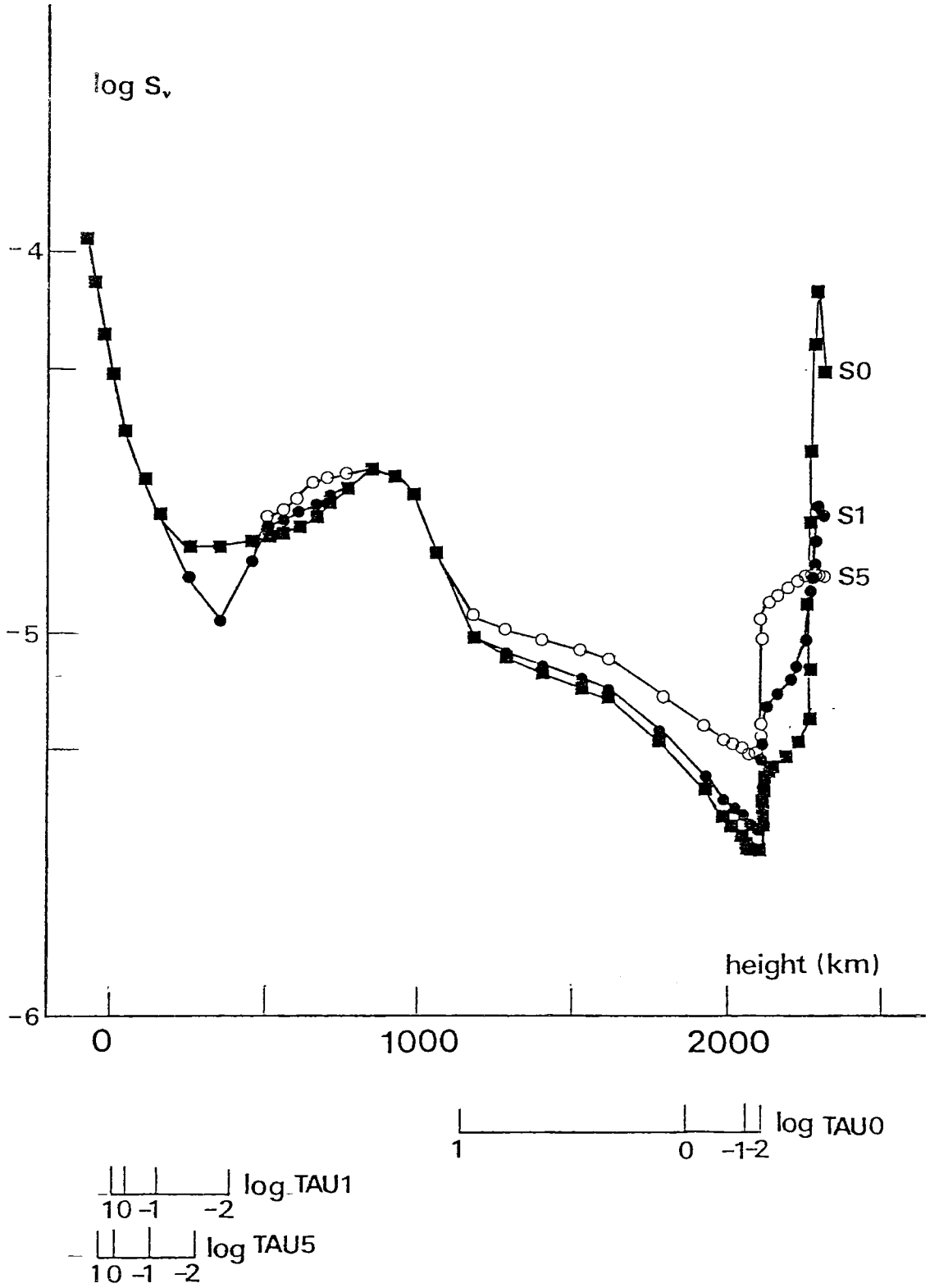
log S_ν
-4
-5
-6
S0
S1
S5
height (km)
0
1000
2000
log TAU0
1
0
-1
-2
log TAU1
10
-1
-2
log TAU5
10
-1
-2

Figure 8

Figure 9

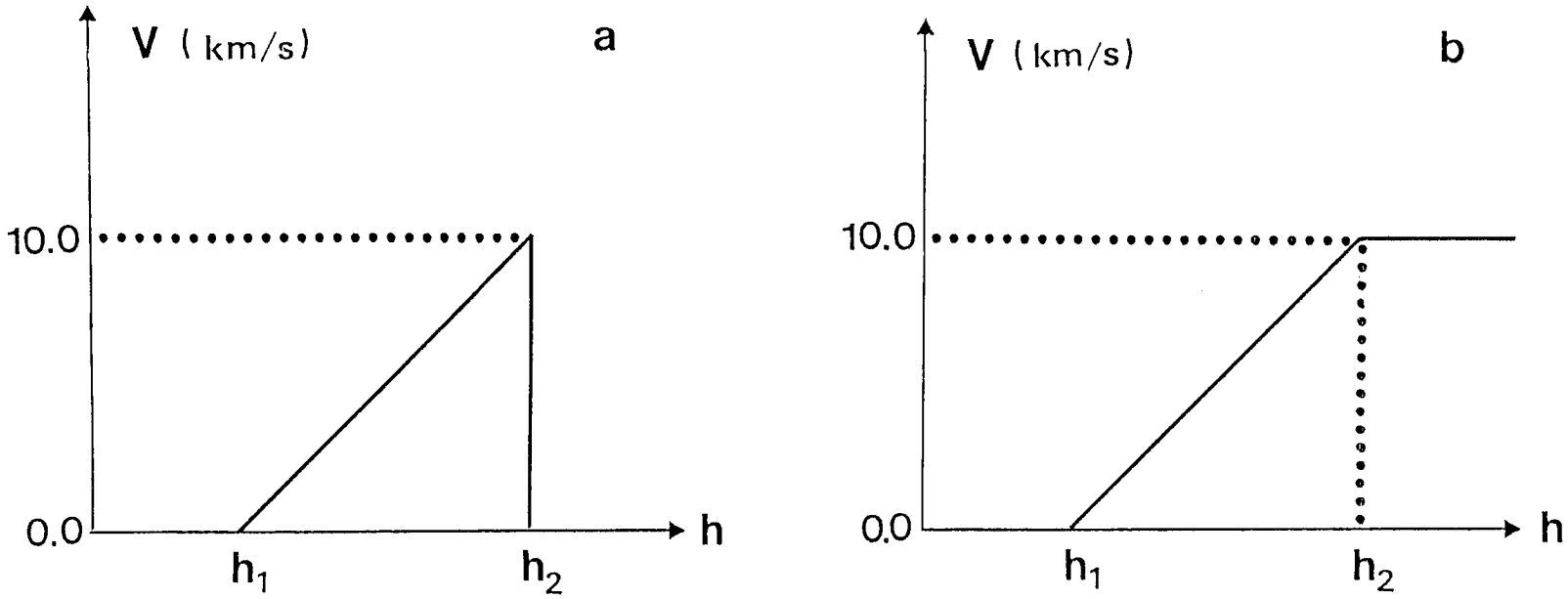

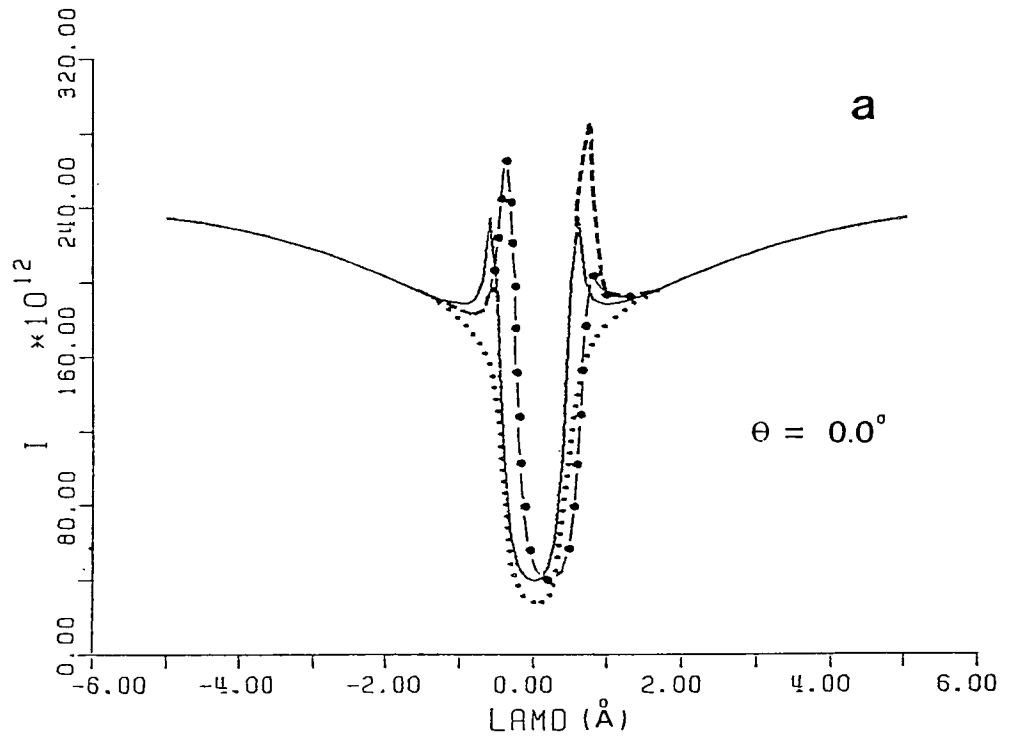
a
θ = 0.0°
I ×10^12
0.00
80.00
160.00
240.00
320.00
-6.00
-4.00
-2.00
0.00
2.00
4.00
6.00
LAMD (Å)

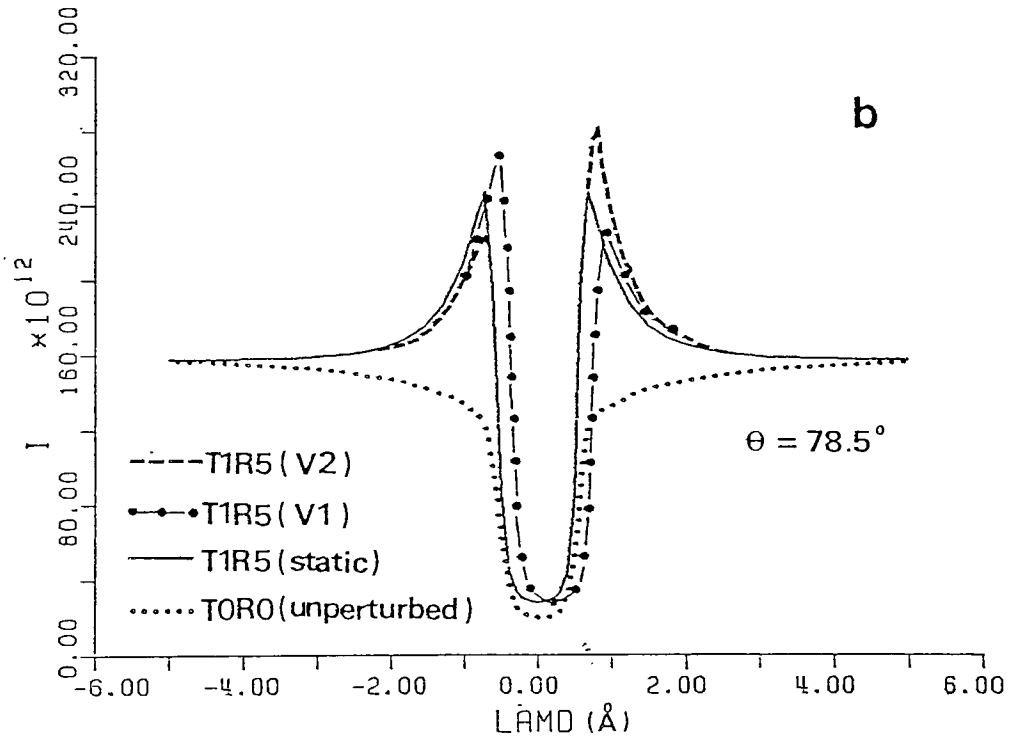
b
θ = 78.5°
T1R5 (V2)
T1R5 (V1)
T1R5 (static)
T0R0 (unperturbed)
I ×10^12
0.00
80.00
160.00
240.00
320.00
-6.00
-4.00
-2.00
0.00
2.00
4.00
6.00
LAMD (Å)

Figure 10

Figure 11

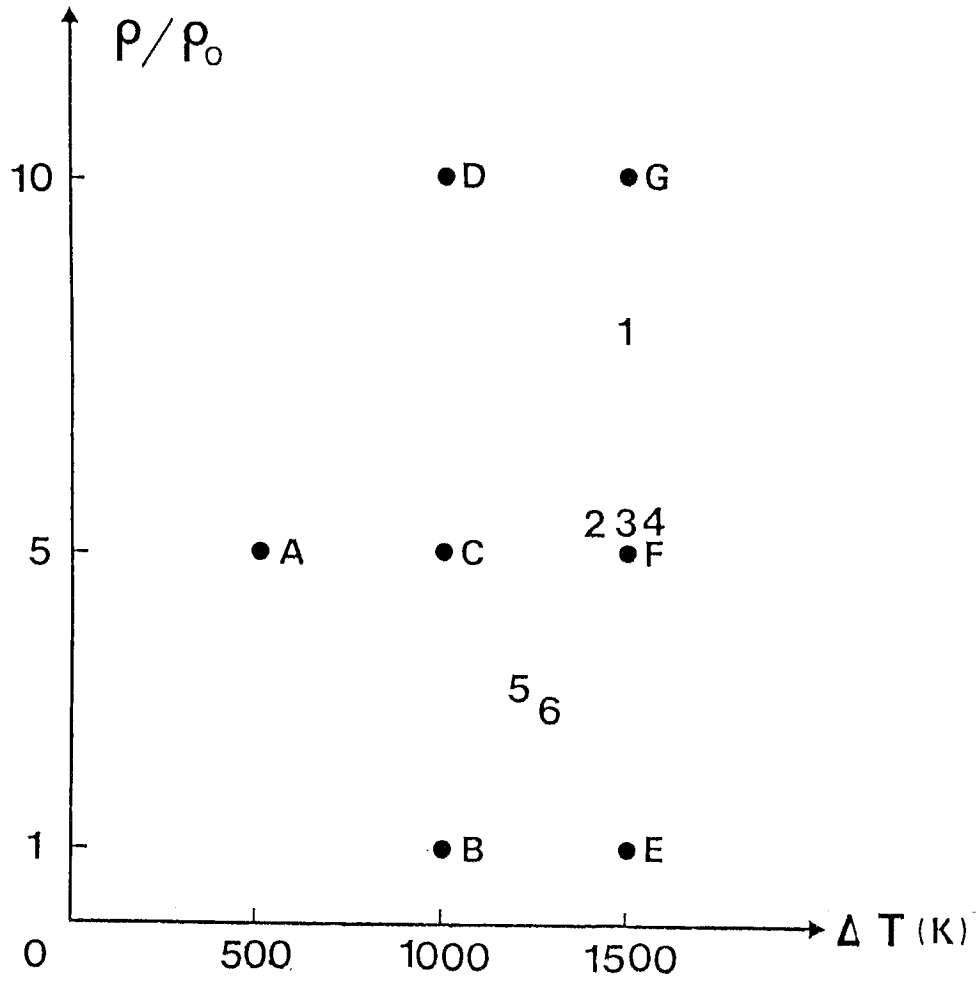

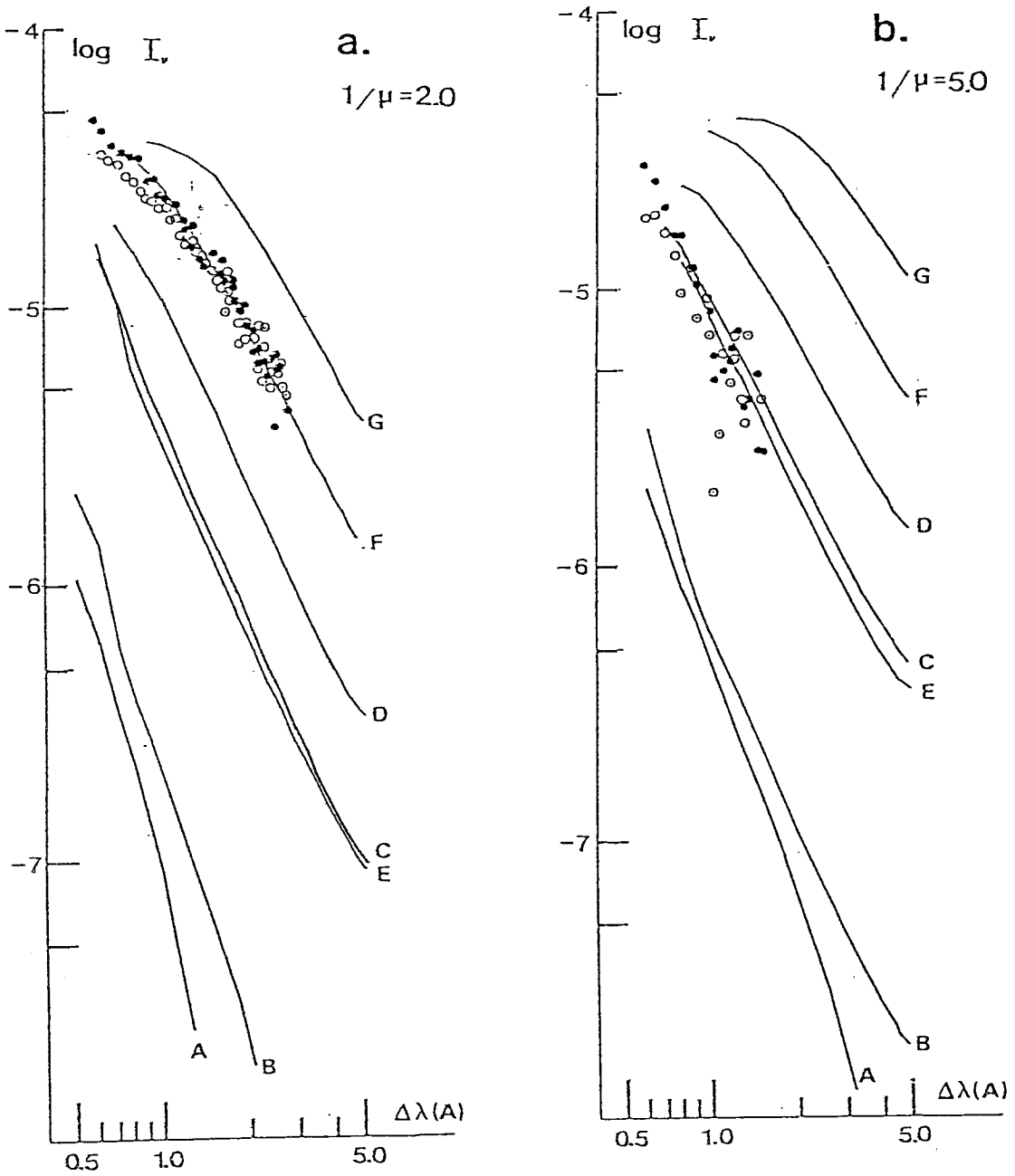
a.
log I,
1/μ=2.0
-4
-5
-6
-7
G
F
D
C
E
A
B
Δλ(A)
0.5
1.0
5.0
b.
log I,
1/μ=5.0
-4
-5
-6
-7
G
F
D
C
E
B
A
Δλ(A)
0.5
1.0
5.0

Figure 12